IOP PUBLISHING NANOTECHNOLOGY
Nanotechnology **18** (2007) 335304 (7pp) doi:10.1088/0957-4484/18/33/335304

Step-mediated size selection and ordering of heteroepitaxial nanocrystals

I Goldfarb

School of Mechanical Engineering, Faculty of Engineering, and University Research Institute for Nanoscience and Nanotechnology, Tel Aviv University, Ramat Aviv, Tel Aviv 69978, Israel

E-mail: ilang@eng.tau.ac.il

Received 12 April 2007, in final form 17 June 2007
Published 25 July 2007
Online at stacks.iop.org/Nano/18/335304

Abstract
It is necessary to control the size, shape, and uniformity of self-assembled and self-organized nanocrystals in order to use them in real devices. The way to achieve this in epitaxial nanocrystal arrays is by manipulating the bulk stress and/or the surface stress. In this work, an additional and fundamentally different mechanism of $CoSi_2$ nanocrystal size selection is reported, based on a preferential reaction of Co adatoms with Si ledge atoms at the step bunches on a vicinal Si(111) surface, where the mean silicide nanocrystal size and nanocrystal–nanocrystal separation distance along the ledge are determined by the step-bunch height. These results may have important implications for the lithography-free fabrication of ordered functional nanostructure ensembles.

1. Introduction

Ever since its discovery in the early 1990s [1–3], spontaneous formation (also known as self-assembly) and ordering (also known as self-organization) of nanometre-size three-dimensional (3D) islands (hereby termed nanocrystals) of perfect geometry and crystal structure on surfaces by heteroepitaxy (strained-layer growth on lattice-mismatched substrates) has been the focus of a great deal of research effort. Self-assembled quantum-well, quantum-wire, and quantum-dot nanostructures are interesting not only from a purely fundamental point of view. Their unique, atom-like electronic structure and properties [4] pave the way to bottom-up made light-emitting devices (LEDs) and lasers [5, 6], single-electron transistors (SETs) [7, 8] and logic gates based on charge or spin quantum-dot cellular automata (QCAs) [9, 10]. In addition, improved catalytic reactions in the presence of metallic nanoparticles on surfaces have been reported [11, 12]. The fabrication of such tiny nanometric devices by a conventional top-down approach is not easily achieved. So far, many efforts have been devoted to group IV elemental (Si, Ge) [13, 14] and II–VI and III–V compound semiconductor nanostructures (especially direct band gap arsenides and antimonides) for photonic applications [4–6]. Yet, the ability of metal and metal-silicide nanostructures to self-assemble in a compact or elongated form [11, 15–17], in conjunction with their room-temperature (RT) Coulomb-blockade and Coulomb-staircase characteristics [18], makes them potential components in single-electron devices. However, using them in real devices requires control over the size, shape, and uniformity of the nanocrystals in the array, and for certain applications, such as QCAs [9, 10], spatial ordering into desired patterns as well.

Perhaps one of the most challenging issues in self-assembly and self-organization is the prevention of Ostwald ripening, where larger nanocrystals grow at the expense of the smaller ones due to the Gibbs–Thomson effect, which tends to reduce the boundary free energy due to higher vapour pressure around it [19, 20]. The problem is that this process creates undesirably broad, negatively skewed nanocrystal size distributions [19]. Homoepitaxial islands are inherently unstable against Ostwald ripening; however, heteroepitaxial ones may be stabilized by the difference in surface stress tensors between them and the substrate, which leads to force multipoles at the boundary between them and resistance to ripening even if the mismatch is very low [4]. If sufficiently high (at least a few per cent) mismatch is present, the growth can be self-limiting because the barrier to adatom attachment to the growing nanocrystal due to the strained ribbon at the nanocrystal–substrate contact region [21] scales with the island size [22, 23]. Either way, the size and separation distance of heteroepitaxial nanocrystals are determined by elastic interactions. Nanocrystals interact repulsively with each other through the substrate, and this strain-dependent repulsion controls the mean separation distance between

them [24]. A better, although more complex, way not only to fix the nanocrystal size, but the mean separation distance and ordering, is by growing strained multilayered nanocrystal superlattices [25, 26], where the nanocrystals interact both in plane and out of plane with neighbours in adjacent layers. Consequently, vertically and spatially correlated nanocrystals can result [25, 26]. In this case, too, the major role is played by the elastic interactions.

In this research effort, an entirely different mechanism of nanocrystal size selection is demonstrated, where the major role is played by the localized kinetics of the Co–Si reaction at a stepped Si surface, rather than by elasticity, with the Si atoms for the reaction with Co adatoms supplied almost exclusively by the steps in the bunches ('staircases' or 'trains'), resulting in a close match between the size of the so-formed $CoSi_2$ nanocrystals and their parent bunch height. Furthermore, clear correlation between these nanocrystal sizes and their respective separation distances along a parent step-bunch ledge was evident, indicating a degree of one-dimensional self-organized ordering.

2. Experimental details

The silicon surface used in this work was vicinal Si(111), where straight and periodic step or step-bunch structures can be well controlled, by varying the magnitude and direction of the heating current during preparatory high-temperature flashes [27]. (In addition, $CoSi_2$ nanocrystal elongation on the Si(001) substrates is avoided.) The experiments were performed in an ultra-high vacuum (UHV, base pressure 1×10^{-8} Pa) variable-temperature scanning tunnelling microscope (STM) (Omicron NanoTechnology GmbH), equipped with reflection high-energy (RHEED) and low-energy (LEED) electron diffraction facilities and an Auger spectrometer. Chemically degreased Si(111) wafers were repeatedly flashed in UHV at about 1150 °C and slowly cooled to RT, as measured with an infrared pyrometer with estimated ±30 °C accuracy. This preparation resulted in a well-ordered bunched (7×7) surface (observed in RHEED, LEED, and STM), with 87.4 ± 9.7 nm mean bunch period, 6.6 ± 1.0 nm mean bunch height, and mean 4.3°-miscut, as shown in figures 1(a) and (b). Sub-monolayer Co coverage was slowly evaporated at RT from a precise e-beam evaporator onto the flashed surface mounted in the STM stage, and subsequently underwent annealing cycles up to 550 °C in the STM, to promote the silicide formation, while being constantly imaged in real time. All the STM images shown in this work were acquired in constant-current mode with 0.15 nA tunnelling current.

3. Results and discussion

3.1. Nanocrystal formation at the steps and step bunches of Si surfaces

The Co/Si(111) layer evolution is shown in figure 1. Since it is convenient to visualize and analyse certain features in a topographic mode, but others in a current mode, the upper halves of the frames in figures 1(b)–(e) are current images, whereas the lower ones are topographic (a similar mixed-mode representation appears in figures 7(a), (c), and (e)). At

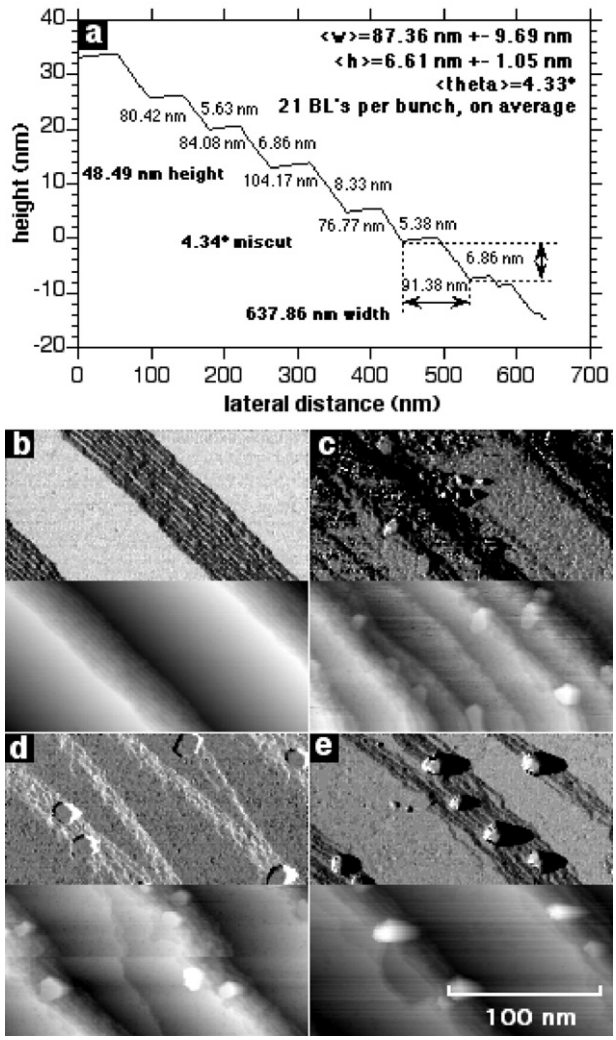

Figure 1. STM sequence of Co evolution on a stepped Si(111) surface. (a) Typical height profile scanned across periodic step bunches on the surface. (b) Step bunches on the Si(111) surface prior to the deposition of cobalt, with individual ledges in the bunch resolved. $V_t = -0.5$ V. (c) Flat two-dimensional $CoSi_2$ platelets begin to form, extending from the step bunches at 400 °C ($V_t = -0.7$ V), and (d) their formation seems complete at 450 °C ($V_t = -0.5$ V). (e) Three-dimensional nanocrystal formation in the course of a 3 h anneal at 500 °C. $V_t = +0.7$ V.

400 °C first silicide nanocrystals are formed (see figure 1(c)). At this stage, they are still small and flat two-dimensional (2D) polygonal platelets growing out of individual steps in the bunch and, since Co atoms are not yet consumed (see tiny Co agglomerates in the top part of figure 1(c)), the nucleation process continues and competes with growth. This secondary nucleation diminishes at 450 °C, where Co agglomerates could no longer be detected (figure 1(d)), and the growth stage progresses with annealing time, culminating at a thickening transition into hemispherical shape, signalling a completion of the three-dimensional (3D) $CoSi_2$ nanocrystal formation process at 500 °C, as shown in figure 1(e).

The transition from 2D to 3D $CoSi_2$ nanocrystals can be understood from figure 2, where in (a) three discrete nucleation events are seen, each at a different step within the same bunch.

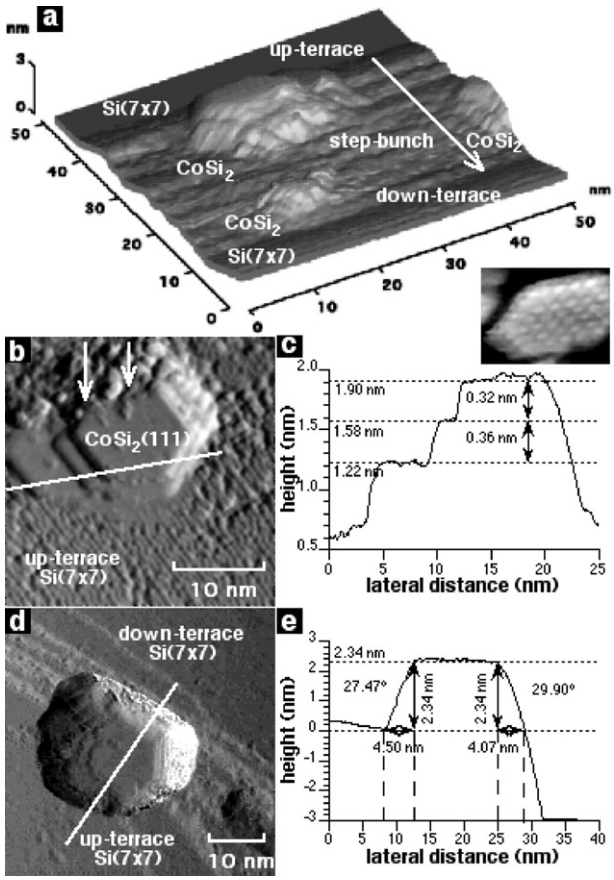

Figure 2. Formation of 3D $CoSi_2$ nanocrystals at the (111) step bunches. (a) 3D view of the formation of stacked $CoSi_2$(111) terraces on a step bunch. The inset shows an atomic-resolution STM image of the top hexagonal $CoSi_2$111)-(2 × 2) terrace. (b) Top view of the upper $CoSi_2$ stack in (a). Si(111)-(7 × 7) reconstruction of the up-terrace is clearly resolved. (c) Height profile along the line in (b), showing the measured heights of the stacked bilayers. (d) Faceted 3D nanocrystal with the stacked bilayers resolved in the right-hand facet, whose cross section along the line is shown in (e). (a) $V_t = +1.0$ V, (b) $V_t = -4.0$ V, and (c) $V_t = -0.7$ V. $T = 500\,^{\circ}$C.

The higher occupation probability of adatoms at steps and step bunches than on terraces is expected in the framework of simple bonding-based models, such as terrace–ledge(step)–kink (TLK or TSK) [20], due to increased coordination (and hence lower surface/interface energy) at the former. Since the 0.309 nm tall $CoSi_2$ (111) bilayers (BLs) are closely matched (∼1.2%) to the 0.313 nm tall Si(111) ones, the formation of vertically stacked 0.31 nm spaced (within the measurement inaccuracy) $CoSi_2$(111) BLs, shown in figures 2(a)–(c), makes perfect sense. The hexagonal symmetry and (2 × 2) reconstruction of the terraces [28] (cf the atomic resolution STM image inset in figure 2(a), with the rhombic unit cell sides of ∼7.6 Å = 2 × $CoSi_2$ ⟨110⟩ interatomic distance), in conjunction with the 0.31 nm BL heights, are clear fingerprints of the fluorite-type $CoSi_2$(111). If similar reasoning is applied to Co on a Si(001) vicinal surface, the formation and stacking of 0.134 nm high monolayers (MLs) in a [001] direction would be expected, as was indeed observed (see figures 3 and 4, respectively).

The BL stacking, step–step interactions, and, most probably, Ehrlich–Schwoebel barrier to crossing the $CoSi_2$ steps [20], may cause BL pile-up and formation of facets bounding 3D nanocrystals, as shown in figures 2(d) and (e). A nanocrystal like that contains at least 7–10 BL stacks above the up-terrace, with twice that number when counting from the flat top to the down-terrace. Neither such tall multiple stacks of 2D terraces (i.e., typically 3–4 stacked bilayers, as in figure 2(b)), nor their transition to 3D faceted nanocrystals, were observed. This, in conjunction with the fact that the interfaces with Si are inclined along the step bunches, whereas the flat tops are parallel to the Si(111) terraces, may indicate thickening by downhill nanocrystal migration (avoiding the nucleation barriers associated with the nucleation of new 2D layers on top of the bottom ones), as has been reported by Ling *et al* [29] and McCarty [30], for Ag and Cu on Ru and W surfaces, respectively. This model is schematically drawn in figure 5. Since the stepped side-wall on the right-hand side of figure 5(a) constitutes easy attachment sites for the downhill migrating atoms, the material from the thinner uphill region (left-hand side in figure 5(a)) is transferred to the thicker downhill region (right-hand side in figure 5(a)). As a result, the island moves to the right and thickens, without the need to overcome the nucleation barriers for every new 2D layer. The case here is more complex, since (i) $CoSi_2$/Si is a Volmer–Weber system, where the wetting layer is absent, and (ii) Co–Si chemical reaction is involved.

On the vicinal Si(001) surface (figure 3(a)) Co adatoms interact with the step edges, as well, more specifically with the ends of dimer rows at S_B and D_B steps, as shown in figure 3(b) and its inset, evolving into 2D $CoSi_2$ platelets (figure 3(c)). S_B and D_B stand for single-height and double-height B-type steps, respectively, whose edges are perpendicular to the up-terrace dimer rows. However, unlike the above described compact $CoSi_2$ platelets on Si(111), due to the two-fold symmetry and anisotropic stress tensor of the (2 × 1) reconstructed Si(001) the platelets are elongated in the ⟨100⟩-directions of the parent dimer rows, as can be seen in figures 3(d) and (e), where a distinct boundary between the parent (2 × 1) dimer rows and the mixed criss-cross (2 × 2)-reconstructed [31, 32] 2D rectangular $CoSi_2$ platelets is apparent (encircled). As in the case of $CoSi_2$/Si(111), stacking of $CoSi_2$(001) terraces is observed, as shown in figure 4 (to be compared with figure 2), only this time these are single (rather than double in the (111) case) 1.34 Å-high layers (marked 'B' in figure 4(a)) that pile up to form full 5.36 Å high unit cells (marked 'A' in figure 4(a)), and they also evolve into 3D nanostructures, as in figure 4(b). Naturally, since the individual 2D components (platelet terraces) are rectangular, so are the final 3D nanostructures, which are elongated in the ⟨100⟩-directions of the platelets. This behaviour clearly renders the Si(001) surface less suitable for self-organization of nanodot arrays.

The rectangular, elongated shape of these (001)-platelets implies that the downhill migrating atoms have to diffuse longer distances to reach the right-hand end of the platelet. This, in conjunction with the fact that 2D nuclei in the both (111) and (001) orientations can be seen growing-out of the individual steps in the bunch (cf the lower-left (111)-island in figure 2(a), and (001)-island in figures 3(c)–(e), respectively), suggest that another mechanism may be responsible for the

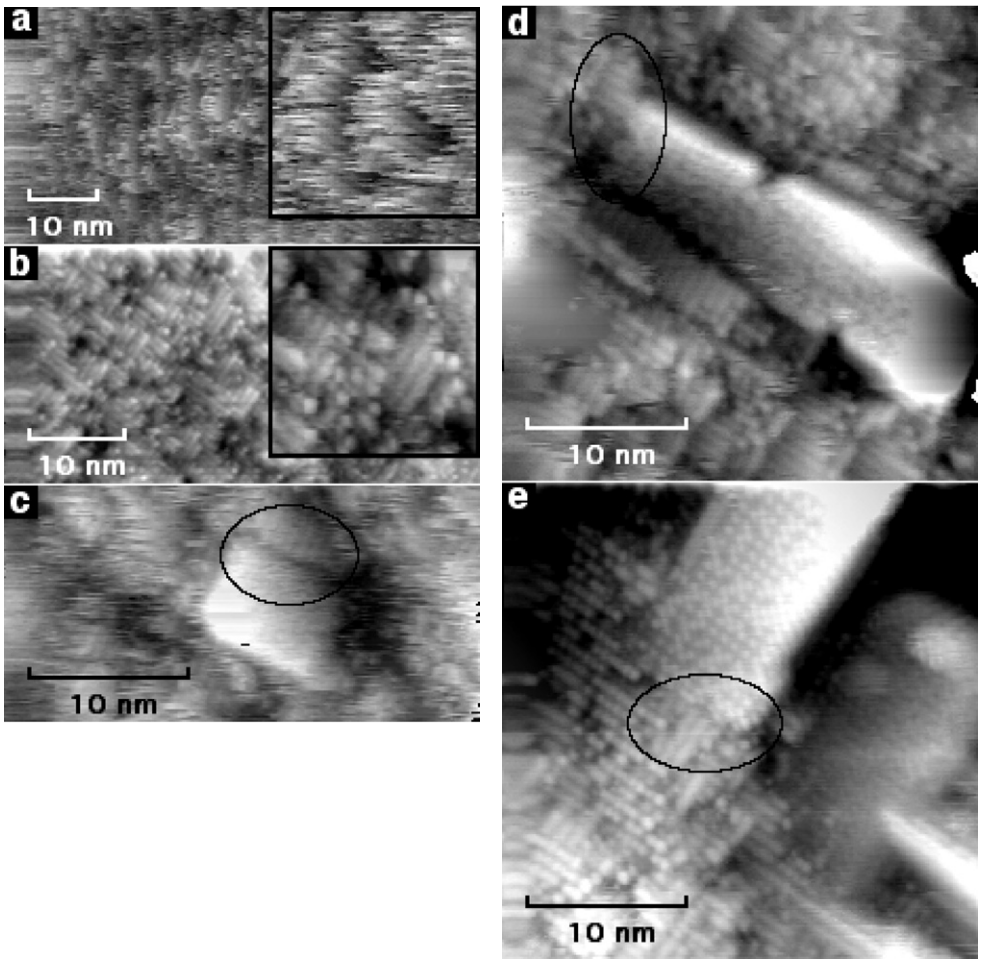

Figure 3. Nucleation and growth of 2D $CoSi_2$ platelets at the 3°-miscut vicinal Si(001) step bunches, where the rough appearance of the double-height steps is caused by the [100]-miscut direction. (a) Pre-deposited surface (magnification in the inset). (b) Nucleation at the dimer-row ends of the D_B and S_B steps (magnified in the inset), and (c) growth and (d) and (e) elongation of 2D $CoSi_2$ platelets. Black ovals encompass the boundary region between the parent dimer rows and the out-growing platelets. The mixed (2×2) and $c(2 \times 2)$ reconstruction, characteristic of $CoSi_2$(001), is clearly seen on the platelet in (e).

step decoration, namely uphill Co diffusion. A plausible model, based on simple TLK arguments [20], is schematically drawn in figures 5(c) and (d). In figure 5(c), Co adatoms and agglomerates are sufficiently mobile to cross the short terraces and climb up the stairs, since their coordination at the bunch ledges is higher than at the on-top terraces, and they preferentially react with Si atoms residing at the bunch ledges. Due to lower coordination at ledge sites these Si ledge atoms are more weakly bonded then Si terrace atoms, and thus more readily available for the reaction there, forming $CoSi_2$ nanocrystals, as schematically shown in figure 5(d). As Si atoms at the uppermost step in the bunch are free to react in both the in-plane (horizontal) and out-of-plane (vertical) direction, many nanocrystals occupy not only the bunch sites, but partially its up-terrace as well, as clearly follows from all the figures shown, and in the high-resolution figure 2, in particular. Initially, flat (probably only one or two {111} bilayers high) platelets are formed at 400–450 °C, extending from the steps, bonded at the edge only, with almost the entire body of the platelet freestanding in vacuum (see figures 1(c), (d) and 2). Such a freestanding morphology should be very beneficial in terms of elastic relaxation of the $CoSi_2$/Si mismatch strain. Figures in this work (figures 1, 6, 7, and especially 2(a)) explicitly show many of the $CoSi_2$ nanocrystals located not only at the up-terrace of the step bunches, but actually occupying a good portion of the bunches themselves (i.e., part of the nanocrystal at the up-terrace with the remaining part spreading over the adjacent down-bunch). These observations disagree with those of Zilani *et al* [33], who claimed that the nanocrystals are pinned to the upper step edges due to Ehlich–Shwoebel barriers against adatoms diffusing down a descending step.

3.2. Late-stage evolution of the silicide nanocrystals

During a 500 °C anneal of the $CoSi_2$ nanocrystals on the Si(111) surface, the so-called 'late-stage growth' seems to begin, where the supersaturation, e.g., concentration of the dilute phase (adatoms), is reduced to such an extent that it is insufficient to drive (a) new nucleation events and (b) growth of the existing clusters by adatom capture from the dilute phase [19]. In such a case, growth becomes a global phenomenon, with the whole cluster distribution interacting through the remaining degree of supersaturation, in a way

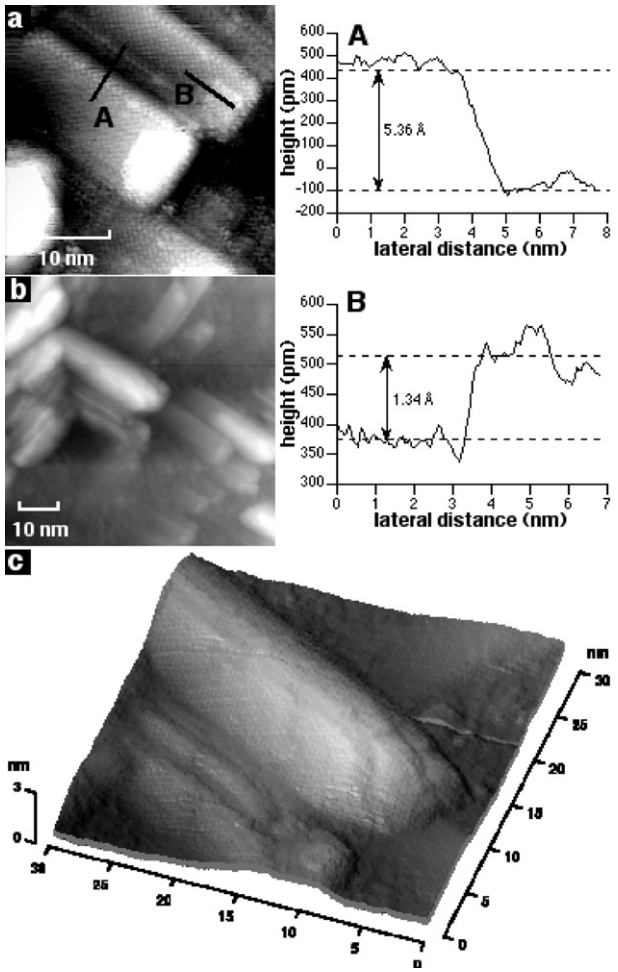

Figure 4. (a) Stacked $CoSi_2$(001)-(2 × 2) monolayers (MLs). The cross-sectional contour height profiles on the right were measured along the black lines, and correspond to (A) an entire fluorite $CoSi_2$(001) unit cell made by stacking of 4 MLs, and (B) a single (001) ML. (b) Faceted 3D $CoSi_2$ nanocrystals, elongating along the [100] and [010] in-plane directions. (c) A 3D view of a typical nanocrystal from the centre of (b).

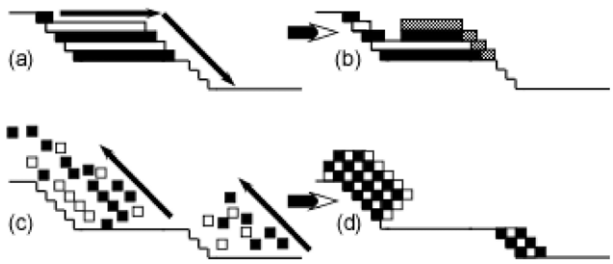

Figure 5. Two plausible models for the formation of $CoSi_2$ nanocrystals at the vicinal Si(111) step-bunches. (a), (b) Downhill migration model, and (c), (d) upward climb model. See text for details.

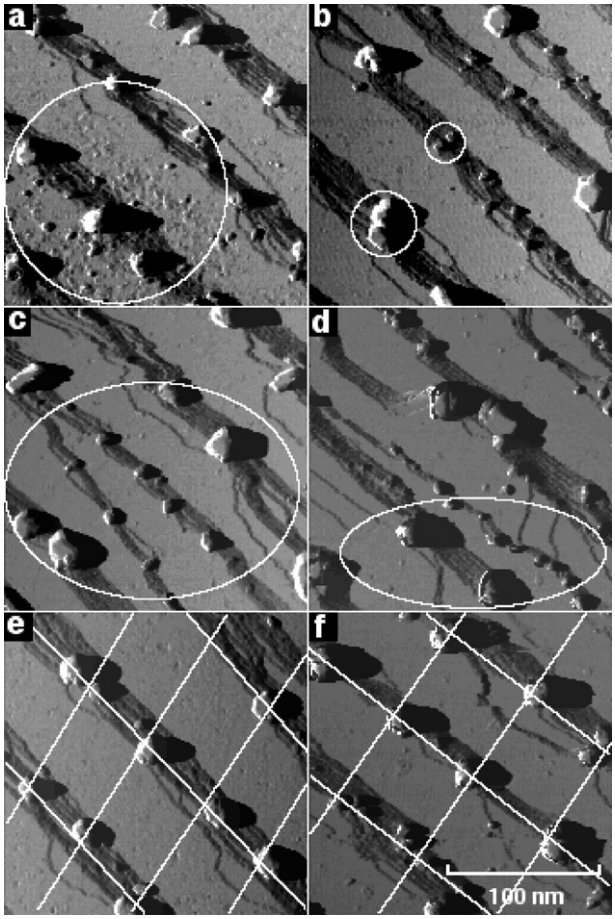

Figure 6. Nanocrystal self-organization and size-selection processes. (a), (b), Nanocrystal coarsening at 500 °C by Ostwald ripening (note material transfer from small dissolving terrace islands towards larger nanocrystals at the step bunches in the centre and bottom-left part of (a)), and coalescence events at the step bunches encircled in (b). $V_t = +2.0$ V. (c), (d) Bunch nanocrystals are stabilized against Ostwald ripening driven dissolution even if they are much smaller than the mean size. (c) $V_t = +2.0$ V. (d) $V_t = +3.0$ V. (e) Nanocrystal evolution after a 3 h annealing treatment at 500 °C. $V_t = +2.0$ V. (f) The vast majority of the nanocrystals at 550 °C fill the entire bunch height. $V_t = +3.0$ V. White lines designate mean nanocrystal periodicity and approximate alignment across the terraces.

that clusters smaller and larger than the mean size are out of balance with the adatom concentration. This imbalance drives the late-stage growth, such that smaller clusters, with a higher equilibrium concentration, contribute atoms to the larger ones (with a lower equilibrium concentration), due to the Gibbs–Thomson effect, also known as Ostwald ripening. Another way to reduce the boundary free energy is by coalescence, i.e., growth of neighbouring clusters into each other, which is another phenomenon usually associated with the late-stage growth [19]. While both Ostwald ripening and coalescence can take place in parallel with nucleation during the early growth stages, they certainly dominate the late growth stages, and can be seen in figures 6(a) and (b), respectively. Ostwald ripening events appear in the bottom-left, encircled part of figure 6(a), where terrace islands dissolve, with the released material transferred towards the bunch nanocrystals, and in figure 6(b) coalescence events at the bunches are encircled. While nanocrystal coalescence takes place at bunches, dissolution due to Ostwald ripening is active on terraces. In other words, only small terrace nanocrystals are destabilized by the larger bunch nanocrystals and are 'sacrificed' in favour of the

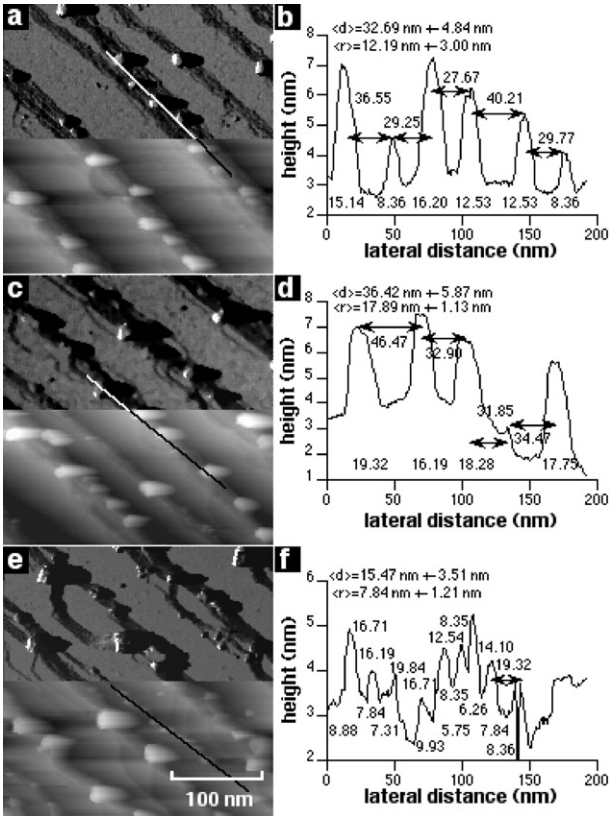

Figure 7. Nanocrystal size and separation distance variation with annealing. (a), (c), and (e), are composed of current images in their upper part, and topography images in the lower part. (b), (d), and (f) show characteristic height profiles taken along the lines drawn in (a), (c), and (e), respectively. (a), (b), Immediately upon formation at 500 °C, (c), (d) after a prolonged anneal at 500 °C, and (e), (f) at 550 °C. (a) $V_t = +0.7$ V, (c) $V_t = -0.3$ V, and (e) $V_t = +3.0$ V.

latter. They can only 'survive' by residing at step bunches, as encircled in figure 6(c) and, in a particularly striking example, in figure 6(d), where really tiny nanocrystals seem to be protected from dissolution by their location at equally low-height parent bunches (only very few can be spotted in the midst of terraces). Those low-height bunches result from occasional branching of the tall, regular ones (whose height is determined by the average miscut angle), or from local step pinning. Both coarsening mechanisms, i.e., Ostwald ripening and coalescence, progressively increase the mean nanocrystal size with annealing time, gradually approaching the size comparable with the bunch height (figure 6(e)). The coarsening continues at 550 °C until the vast majority of nanocrystals attain their maximal size dictated by the parent bunch height, as in figure 6(f).

3.3. Nanocrystal size selection and ordering

At every stage of evolution, the mean nanocrystal size (selected by its parent step bunch) determines the mean nanocrystal–nanocrystal separation distance. Initially, upon 3D formation at 500 °C (few hours), neither the mean size ($\langle r \rangle = 12.19 \pm 3.00$ nm) nor separation ($\langle d \rangle = 32.69 \pm 4.94$ nm) have apparently reached their optimal values (see figures 7(a), (b)), since both continued to evolve with annealing. After prolonged

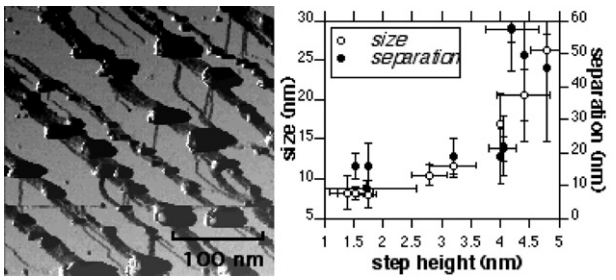

Figure 8. On the right: dependence of the mean nanocrystal size and separation periodicity along the ledges on the step-bunch height, measured from the multiple bunch-height image on the left. Vertical error bars reflect the standard deviation of the mean nanocrystal size and separation periodicity, whereas horizontal bars reflect the standard deviation of the mean step-bunch height.

(few days) and repeated annealing cycles in the 250 °C–500 °C range, both values increased to $\langle r \rangle = 17.89 \pm 1.13$ nm and $\langle d \rangle = 36.42 \pm 5.87$ nm, respectively (figures 7(c), (d)), i.e., a reduction of the size/separation ratio from $\langle d \rangle / \langle r \rangle > 2.5$ to $\langle d \rangle / \langle r \rangle \approx 2$. Furthermore, an identical size/separation ratio of $\langle d \rangle / \langle r \rangle \approx 2$ was also maintained for the small nanocrystals, residing at the lower step bunches, such as the ones shown in figure 6(d), as follows from figures 7(e), (f). While the dispersion, especially in the separation values, is quite large (about 30% for the separations and about 20% for the sizes), these values were obtained by analysing almost 500 nanocrystals (and a similar number of separations) in total, by profiling many tens of nanocrystal rows as shown in figure 7, so the standard errors of the sampling are very small. Hence, the dispersions are genuine, reflecting the on-going self-organization process, namely 1D nanocrystal ordering by step-bunch-mediated size selection, and corresponding nanocrystal–nanocrystal separation along the bunches. Locally, there exist regions on the surface where the nanocrystals are of such a size that the corresponding nanocrystal–nanocrystal separations are comparable with the terrace widths. As shown in figures 6(e) and (f), at those locations 2D ordered patches result.

To present the dependence of the nanocrystal size and periodicity (nanocrystal–nanocrystal separation) along the ledges in a more quantitative manner, a locally less ordered region with a variety of step-bunch heights and, hence, nanocrystal sizes and periodicities was selected, where the nanocrystal sizes and periodicities were measured as a function of their respective mother-bunch heights, as shown in figure 8.

4. Conclusions

In conclusion, a new mechanism for size selection of self-assembled heteroepitaxial nanocrystals is reported, which is not based on elastic interactions. The kinetics of Co–Si reaction on a stepped Si(111) surface is such that the deposited cobalt reacts preferentially with the Si substrate atoms at the bunched steps (rather than terraces). By itself, the step-decoration phenomenon is neither new nor surprising, merely depending on the deposit diffusion length relative to the terrace width. However, the new part here is the fact that the mean size

of the so-formed nanocrystals is determined by their parent-bunch height. Furthermore, the bunch-selected mean size affects the mean nanocrystal–nanocrystal separation distance along the bunch (roughly 1:2 ratio, respectively), creating one-dimensionally periodic structures. The exact reason for the observed size–separation correlation is currently not known. One possible candidate is the mismatch-induced repulsion, although small value of the nominal $CoSi_2$/Si mismatch ($\sim$1.2%) seems somewhat low to account by itself for the rather long-distance interactions (e.g., Si step decoration by a more highly mismatched Ge ($\sim$4.2%) islands did not result in well-defined separation distances along the edge [27]). Yet, in the absence of a better explanation, ordering from overlapping strain fields remains a plausible candidate (cf the reasoning of Wu *et al* for the observed ordering of NiSi nanodots on the undulations and dislocation cross-hatched patterns of relaxed SiGe templates [34]). Localized weaker spatial correlation between the nanocrystal positions is also observed across the terraces, implying that by further reducing the terrace width (to the extent comparable with the nanocrystal–nanocrystal separations) ordered two-dimensional nanocrystal arrays can be created. While two-fold symmetry of the Si(001) surface was transferred to the epitaxial $CoSi_2$ nanostructures, causing anisotropic elongation, the mere fact of a similar step-mediated nanostructure evolution indicated the generic nature of this mechanism, that, hence, should be active in any system where substrate atoms are an integral part of the growing compound islands. These results may have important implications for the non-lithographic bottom-up fabrication of functional nanostructures.

Acknowledgments

The author gratefully acknowledges the contribution of O Becker and M Levinshtein to the experiments.

References

[1] Eaglesham D J and Cerullo M 1990 *Phys. Rev. Lett.* **64** 1943
[2] Mo Y-W, Savage D E, Swartzentruber B S and Lagally M G 1990 *Phys. Rev. Lett.* **65** 1020
[3] Guha S, Madhukar A and Rajkumar K C 1990 *Appl. Phys. Lett.* **57** 2110
[4] Schukin V A, Ledentsov N N and Bimberg D 2004 *Epitaxy of Nanostructures* (Berlin: Springer)
[5] Murray C B, Kagan C R and Bawendi M G 1995 *Science* **270** 1335
[6] Fafard S, Hinzer K, Raymond S, Dion M, McCaffrey J, Feng Y and Charbonneau S 1996 *Science* **274** 1350
[7] Alivisatos A P 1998 *MRS Bull.* **23** 19
[8] Repp J, Meyer G, Olsson F E and Persson M 2004 *Science* **305** 493
[9] Orlov A, Amlani I, Bernstein G H, Lent C S and Snider G L 1997 *Science* **277** 928
[10] Imre A, Csaba G, Ji L, Orlov A, Bernstein G H and Porod W 2006 *Science* **311** 205
[11] Valden M, Lai X and Goodman D W 1998 *Science* **281** 1647
[12] Lauritsen J V, Nyberg M, Nørskov J K, Clausen B S, Topsøe H, Lægsgaard E and Besenbacher F 2004 *J. Catal.* **224** 94
[13] Medeiros-Ribeiro G, Bratkovski A M, Kamins T I, Ohlberg D A A and Williams R S 1998 *Science* **279** 353
[14] Ross F M, Tromp R M and Reuter M C 1999 *Science* **286** 1931
[15] Goldfarb I and Briggs G A D 1999 *Phys. Rev.* B **60** 4800
[16] Goldfarb I, Cohen-Taguri G, Grossman S and Levinshtein M 2005 *Phys. Rev.* B **72** 075430
[17] Chen Y, Ohlberg D A A and Williams R S 2002 *J. Appl. Phys.* **91** 3213
[18] Oh J, Meunier V, Ham H and Nemanich R J 2002 *J. Appl. Phys.* **92** 3332
[19] Zinke-Allmang M, Feldman L C and Grabow M H 1992 *Surf. Sci. Rep.* **16** 381
[20] Zhang Z and Lagally M G 1997 *Science* **276** 377
[21] Shklyaev O E, Beck M J, Asta M, Miksis M J and Voorhees P W 2005 *Phys. Rev. Lett.* **94** 176102
[22] Jesson D E, Chen K M and Pennycook S J 1996 *MRS Bull.* **21** 31
[23] Jesson D E, Chen G, Chen K M and Pennycook S J 1998 *Phys. Rev. Lett.* **80** 5156
[24] Johnson H T and Freund L B 1997 *J. Appl. Phys.* **81** 6081
[25] Tersoff J, Teichert C and Lagally M G 1996 *Phys. Rev. Lett.* **76** 1675
[26] Springholz G, Holy V, Pinczolits M and Bauer G 1998 *Science* **282** 734
[27] Sgarlata A, Szkutnik P D, Balzarotti A, Motta N and Rosei F 2003 *Appl. Phys. Lett.* **83** 4002
[28] Ilge B, Palasantzas G, de Nijs J and Geerligs L J 1998 *Surf. Sci.* **414** 279
[29] Ling W L, Giessel T, Thürmer K, Hwang R Q, Bartelt N C and McCarty K F 2004 *Surf. Sci.* **570** L297
[30] McCarty K 2006 *Nano Lett.* **6** 858
[31] Stalder R, Schwarz C, Sirringhaus H and von Känel H 1992 *Surf. Sci.* **271** 355
[32] Zilani M A K, Liu L, Xu H, Feng Y P, Wang X-S and Wee A T S 2006 *J. Phys.: Condens. Matter* **18** 6987
[33] Zilani M A K, Xu H, Wang X-S and Wee A T S 2006 *Appl. Phys. Lett.* **88** 023121
[34] Wu W W, He J H, Cheng S L, Lee S W and Chen L J S 2003 *Appl. Phys. Lett.* **83** 1836